

Low load operating protocol investigation of a 620MWe power boiler using an indirectly coupled process model

B.T. Rawlins, R. Laubscher*, P. Rousseau

Department of Mechanical Engineering, Applied Thermal-Fluid Process Modeling Research Unit, University of Cape Town, Library Rd, Rondebosch, Cape Town, 7701, South Africa

Abstract

Low load operation of utility boiler

Keywords: CFD, Eulerian-Eulerian, Boiler, Low-load operation

Nomenclature

<i>Symbol</i>	<i>Quantity</i>	<i>Unit</i>
A	Area	m^2
A_p	Particle surface area	m^2
d_p	Particle diameter	m
E	Fluid total energy	J/kg
E_a	Reaction activation energy	$J/kmol$
P	Pressure	Pa
T_g	Gas temperature	K
T_p	Particle temperature	K
u	Velocity	m/s

1. Introduction

The use of coal fired power plants (CFPP) to provide electricity generation
5 is intended to be phased out in order to mitigate the ingress of climate change.

*Corresponding author

Email address: `ryno.laubscher@uct.ac.za` (R. Laubscher)

However, the switch to more sustainable generation sources pose great challenges for developing countries due to the long transition times and costs involved [1]. Due to the abundance of coal resource present in South Africa CFPPs are the dominant power generation source, with approximately 80 % of the energy needs
10 being met using CFPPs [2]. The promising integration of renewable energy and the decommissioning of old CFPPs in South Africa, will push CFPP from a primarily base load operation to a mid-merit/flexible operating protocol. This will inherently mean CFPPs will need to operate at low-loads for continuous time periods.

15 Mathematical models that can accurately capture the behaviour of the boilers thermal-hydraulic response at varying loads can be used to determine the safe and efficient operating limits [3]. Since, the long term deviation from design conditions can lead to operational incapacibilities affecting combustion stability [4], an increase in harmful emissions [5] and the localised overheating of heat
20 exchangers due to insufficient cooling being provided by the internal working fluid [6].

The full scale testing or experimentation of CFPPs is deemed to expensive to pursue, thus the use of computational fluid dynamics (CFD) allows for the modelling of a full-scale CFPPs, at steady-state, to be investigated at various
25 loads circumnavigating the use of time-consuming and costly field tests. CFD simulations have been successfully used to model a variety of CFPP boiler types ([7], [8]) and cover various aspects such as pollution control ([9],[10]), gas-solid flow effects ([11]) and boiler retrofitting ([8], [12]).

Recent CFD studies investigating low-load operation of CFPP boilers have
30 focused on the combustion stability, harmful emissions and the gas flow-solid flow interactions [13]. The works of Belosevic et al [14] found that the low-load operation of boiler considerably affect the flow and temperature fields, the flame geometry, chemical reactions and concentrations of combustion products.

Hernik et al [4] investigated the effects of using different mill system configurations at a minimum boiler load of 40 %. The most favourable mill system
35 configuration was selected based on the case that exhibited suitable combustion

stability and emission of harmful substances. Similarly, Chang et al [5] investigated the various firing arrangements of a 630 *MWe* tangentially fired boiler. A burner angle of -15° was found to be the optimal arrangement resulting in
40 the best compromise in combustion stability and lower emissions. However, to the best the authors' knowledge, no integration of 1-D thermal-hydraulic model has been used to investigate the steam side operational performance of a CFPP boiler at low-load.

The use of a 1-D thermal-hydraulic modelling approach have been used by re-
45 searchers to investigate the water and gas side heat transfer interactions. These studies are usually used to investigate a transient event, such as a sudden disturbance, start-up or boiler load ramping [15]. Due to the non-uniformities found in CFPP furnaces which are composed of complex combustion dynamics, gas-solid interactions and radiation heat transfer phenomena, 1-D thermal-hydraulic
50 models can not resolve the fireside with sufficient accuracy, but can adequately resolve the waterside energy and momentum transport in a computationally inexpensive manner.

The use of coupled simulations has proven to solve the deficiencies of a full 1-D thermal-hydraulic model by coupling the fireside CFD to a 1-D water
55 network. Recently Laubscher and Rousseau [16] conducted a comprehensive numerical study on the impact of particle radiation properties for high ash coals using ANSYS Fluent v19.2[®] and Flownex SE[®]. Yu et al [17] used a coupled simulation methodology to estimate the superheater (SH) metal temperatures of a 660 *MWe* tangentially-fired coal boiler.

60 The current work proposes the use of CFD modelling methodology to investigate the low-load operational combustion conditions and optimal burner firing arrangement of 620 *MWe* two-pass sub-critical boiler. Furthermore a process model of boilers entire system, including the furnace up till the secondary air-heater, was modelled, which was indirectly coupled to the CFD model, to
65 investigate the necessary process controls needed to ensure; an adequate boiler utilization efficiency, sufficient supply of attemperation/cooling of the radiant SH's and an exit main steam temperature supply of $535^\circ C$.

The model was simulated for a 32 % boiler load with 6 various firing combinations. To establish the accuracy of the CFD modelling approach a validation study was conducted for 100 %, 80 % and 60 % boiler loads and compared to plant measurements to quantify the model accuracy, this is highlighted in section 4.1 prior to the results of the low-load study.

2. Mathematical model

In this section the modelling techniques used by the study are elaborated. A description of the CFD modelling configuration is discussed focusing on the fluid flow, turbulence and combustion modelling as well as the particle transport field resolution. Following this is a description of the adopted heat transfer modelling techniques and the ends with a description of the process modelling configuration.

2.1. Computational fluid dynamics modelling

2.1.1. Fluid flow, turbulence and combustion modelling

The flue gas was modelled using a Eulerian framework. The species transport modelling approach was used to approximate the mixture of chemical species in the gas phase. This approach solves a species continuity equation for each constituent present in the mixture. To reduce the computational burden it was assumed that the various processes were in steady-state. The governing equations for the gas phase can be written as follows;

Mass conservation:

$$\frac{\partial}{\partial x_i}(\rho \bar{u}_i) = S_m. \quad (1)$$

Momentum conservation:

$$\frac{\partial}{\partial x_i}(\rho_{eff} u_i u_j) + \frac{\partial \bar{P}}{\partial x_j} = \frac{\partial}{\partial x_i} \left[\mu \left\{ \frac{\partial u_j}{\partial x_i} + \frac{\partial u_i}{\partial x_j} - \frac{2}{3} \delta_{ij} \frac{\partial u_i}{\partial x_i} \right\} \right] + \frac{\partial}{\partial x_i}(-\rho \overline{u'_i u'_j}) + S_m \quad (2)$$

Energy conservation:

$$\frac{\partial}{\partial x_i}(u_i[\rho E + P]) = \frac{\partial}{\partial x_j} \left[\lambda \frac{\partial T_g}{\partial x_j} \right] + S_h \quad (3)$$

Species transport:

$$\begin{aligned} \frac{\partial}{\partial x_i}(\rho u_j Y_k) &= -\frac{\partial}{\partial x_j}(\vec{J}_k) + \sum_r R_{j,r} + S_k \\ k &= 1, 2, 3 \dots N \end{aligned} \quad (4)$$

To correctly account for the particle inertial effects on the gas phase convection an effective density is defined as follows;

$$\rho_{eff} = \frac{\rho \rho_p (\phi_{mp} + 1)}{\rho \phi_{mp} + \rho_p} \quad (5)$$

In the present study the realizable k- ϵ turbulence model was utilized to address the turbulence closure problem. This model has been successfully used by researchers ([14],[7] and [6]), in modelling the effects of coal-fired swirl burners. 85 The model generally generates higher accuracy results, when compared to the standard k- ϵ model, for problems incorporating swirling and separating flows.

The process of coal combustion comprises four steps. Namely, inert heating and evaporation of moisture, devolatilization, char oxidation and gas phase reactions. Equations (2) and (3) show the single rate kinetic model utilized in this study, to model the devolatilization process.

$$\frac{dm_{vol}}{dt} = R_{vol}(m_{0,vol} - m_{vol}) \quad (6)$$

$$R_{vol} = A_{vol} \exp \left(\frac{E_{a,vol}}{RT_p} \right) \quad (7)$$

$$A_{vol} = 2 \times 10^5 [s^{-1}] \quad E_{a,vol} = 6.7 \times 10^7 [J/kmol]$$

A devolatilization temperature of 553 [K] [18] along with the kinetic parameters (equation 3) of Sheng et al [19] were utilized. The char oxidation process is modelled using the diffusion-kinetics limited model developed by Baum and

Street ([20]), which is given in equation (4). The product species of the char oxidation reaction was set to CO as shown in equation (5).

$$\frac{dm_{char}}{dt} = -A_p P_{O_2} \frac{R_{diff} R_c}{R_{diff} + R_c} \quad (8)$$



The diffusion and kinetic rates of equation (4) are defined in equations (6) and (7) with the kinetic parameters again taken from the works of Sheng et al [19].

$$R_{diff} = \frac{5 \times 10^{-12}}{d_p} \left(\frac{T_g + T_p}{2} \right)^0 .75 \quad (10)$$

$$R_c = A_c \exp \left(\frac{E_{a,c}}{RT_p} \right) \quad (11)$$

$$A_c = 0.0053 [kg/m^2 s Pa] \quad E_{a,c} = 8.37 \times 10^7 [J/kmol]$$

The turbulence-chemistry interactions of the gas phase reactions were approximated using the eddy-dissipation-finite rate model used in ANSYS Fluent v19.5[®] which calculates three rates, namely chemical reaction rate, turbulent
90 production eddies dissipation rate and reaction eddies dissipation rate, and uses the minimum of the three for the source terms calculations. A description of the CFD gas phase reactions of the boiler under consideration, using the same coal, was previously published in the works of Laubscher and Rousseau [3].

2.1.2. Particle modelling

95 The particles are modelled using a Eulerian reference frame, similar to the studies of Knaus et al [21] and Benim et al [22], who both successfully used a multi-phase Eulerian-Eulerian (EE) model the characteristics of coal combustion and furnace heat transfer with adequate accuracy. The pseudo particles transported into the domain are modelled using the general scalar field trans-
100 port equation [23]. The pseudo-particles scalar fields are used to define the fuel characteristics based on the proximate analysis composition, namely consisting of moisture, volatile matter, fixed carbon and ash. Each of the scalar field equations are given in table 1.

Table 1: Scalar field equation descriptions

Variable	Description	Transport equation
ϕ_{mp0}	Original/initial mass of particles	$\frac{\partial}{\partial x_i}(\rho u_i \phi_{mp0}) = 0$
ϕ_M	Moisture present in particles	$\frac{\partial}{\partial x_i}(\rho u_i \phi_M) = \frac{1}{V} \frac{dm_{evap}}{dt}$
ϕ_{VM}	Volatile matter present in particles	$\frac{\partial}{\partial x_i}(\rho u_i \phi_{VM}) = \frac{1}{V} \frac{dm_{vol}}{dt}$
ϕ_{FC}	Fixed carbon present in particles	$\frac{\partial}{\partial x_i}(\rho u_i \phi_{FC}) = \frac{1}{V} \frac{dm_c}{dt}$
ϕ_{ASH}	Ash present in particles	$\frac{\partial}{\partial x_i}(\rho u_i \phi_{ASH}) = 0$
ϕ_{hp}	Enthalpy of particle	Equation (8)

The energy transport of the pseudo particle, is transported by defining the particle enthalpy using the following equation:

$$\frac{\partial}{\partial x_i}(\rho u_i \phi_{hp}) = \left(f_{heat} \frac{dM_c}{dt} h_{rxn} + \dot{Q}_{rad} + \dot{Q}_{conv} - \frac{dM_{evap}}{dt} h_{fg} \right) \frac{1}{V} \quad (12)$$

The equation accounts for all the processes associated with energy transport to the particle, namely convection (\dot{Q}_{conv}), radiation (\dot{Q}_{rad}), latent heat ($\frac{dM_{evap}}{dt} h_{fg}$) and near surface char oxidation ($f_{heat} \frac{dM_c}{dt} h_{rxn}$). This gives the model the ability to track the particle temperature in the domain, moving the model away from the thermal equilibrium approach incorporated by previous studies using an EE approach ([22], [24] and [25]). The particle temperature is important in describing the sequential steps found in modelling combustion processes, especially at low boiler loads where mixing and ignition become problematic.

2.2. Heat transfer modelling modelling

The radiation heat transfer is the dominant form of heat transfer found in industrial furnaces [26] and is solved by applying the gray-participating-gas and particle medium configuration of the radiation transport equation (RTE) [27] shown in equation (9).

$$\frac{dI(\vec{r}, \hat{s})}{ds} = \alpha_g \frac{\sigma_S B T_g^4}{\pi} - (\alpha_g + \alpha_p + \sigma_p) I(\vec{r}, \hat{s}) + \frac{\sigma_p}{4\pi} \int_{4\pi} I(\vec{r}, \hat{s}) \Phi d\Omega \quad (13)$$

In the present work the RTE is solved using the P1 model. Ranade and Gupta [18] illustrated minimal differences between the two common radiation models (namely the P1 and discrete ordinates (DO)) for the resultant wall heat transfer rate values when modelling a 210 MWe CFPP boiler. The P1 radiation model can include the effects of particle absorption (α_p) and scattering (σ_p) as well as gas mixture absorption (α_g). The P1 model transport variable is the incident radiation (G - [W/m^2]), and can be written for a particle laden domain as:

$$\frac{\partial}{\partial x_i} \left(\Gamma \frac{\partial G}{\partial x_i} \right) = (\alpha_g + \alpha_p) G - 4 (\alpha_g \sigma_{SB} T_g^4 - \pi E_p) \quad (14)$$

$$\Gamma = \frac{1}{\alpha_g + \alpha_p + \sigma_p}$$

The flue gas absorptivity was calculated using the domain based weighted sum of gray gas model (WSGGM) using the coefficients determined by Smith et al [28]. The WSGGM accounts for the radiation emitted by tri-atomic gases, namely CO_2 , H_2O and SO_2 present in the flue gas stream. The Eulerian description of the terms α_p , σ_p and E_b are determined using the effective number of particles (N_p) present in a cell. Their formulations are given in equations (11) through (13).

$$\alpha_p = \frac{\epsilon_p A_{pn} N_p}{V} \quad (15)$$

$$\sigma_p = \frac{(1 - \epsilon_p)(1 - f_p) A_{pn} N_p}{V} \quad (16)$$

$$E_p = \frac{\epsilon_p \sigma_{SB} T_p^4 A_{pn} N_p}{V} \quad (17)$$

It is important to note that variable properties for (ϵ_p) and (f_p) are used, that
115 are based on the correlations of Lockwood et al [29] and Yin [30] respectively.

2.3. Process simulation model

A 1D discretized model of the furnace evaporator, platen SH, final SH, and subsequent down stream heat exchanging components was developed using Flownex SE[®] 2021. The model simulates the internal convection heat transfer inside the tubes, the conduction through the tube walls. The model is able to simulate the attemperation flows and momentum transport through

the steam/water circuit. The heat exchangers were modelled using a two-phase mixture approach, this assumes that the fluid properties, phase velocities and temperatures are uniform per cross-sectional area. The homogeneous mixture fraction and mixture density are defined in equations (14) and (15) respectively.

$$\alpha_H = \frac{\rho_l x}{\rho_l x + \rho_g(1 - x)} \quad (18)$$

$$\rho_M = (1 - \alpha_H)\rho_l + \alpha_H\rho_g \quad (19)$$

Applying the mixture density the following transport equations are solved;

$$\frac{\partial}{\partial t}(\rho_M A) + \frac{\partial}{\partial s}(\rho_M Au) = 0 \quad (20)$$

$$\frac{1}{A} \frac{\partial}{\partial t}(\rho_M Au) + \frac{1}{A} \frac{\partial}{\partial s}(\rho_M Au^2) = -\frac{\partial p}{\partial s} - \frac{\tau_w P}{A} - \rho_M g \frac{\partial z}{\partial s} \quad (21)$$

$$\begin{aligned} \frac{\partial}{\partial t}(\rho_M h_M) + \frac{1}{A} \frac{\partial}{\partial s}(\rho_M Au h_M) + \frac{1}{2} \frac{\partial}{\partial s}(\rho_M u^2) + \frac{1}{2A} \frac{\partial}{\partial s}(\rho_M Au^3) = \\ \frac{\partial p}{\partial t} + \frac{\dot{Q}_w}{V} - g\rho_M u \frac{\partial z}{\partial s} \end{aligned} \quad (22)$$

The CFD heat load results for the furnace, platen and final SH walls were used as inputs the process model as seen in Figure 2.

120 The process model is used to determine the required attemperation flow rates in order to achieve the exit steam conditions, the boiler efficiency, and the steam generated for each case. The results of this model aid in determining the best firing combination of burner rows for continuous low-load operation, and the effects the various cases have on the system.

125 3. Case study boiler description & set-up

In this section the numerical model configuration, for both the CFD and process model, will be explained, covering the boilers geometry, the process model set-up, the various modelling inputs (e.g. fuel characteristics and boundary conditions) and ends with the numerical solution strategy.

3.1. Geometry & process model set-up

The modelled boiler is a two-pass sub-critical power boiler with a furnace depth of 13.77 [m], a width of 14.01 [m] and a height of 64 [m]. The CFD geometric model (of Figure 1) makes use of a symmetry plane at half the width of the furnace. This was done to reduce the cell count of the numerical mesh.

Both the platen and final SH are modelled as walls, with transverse pitches of 1.143 [m] and 0.8 [m] respectively. There are three levels of burners located on both the front and rear walls at heights of 11.9 [m], 19.3 [m] and 26 [m]. Figure 1 shows the modelled half of the furnace along with the locations of the platen SH, final SH, boundary walls (front, rear and side) and the domains outlet and inlets.

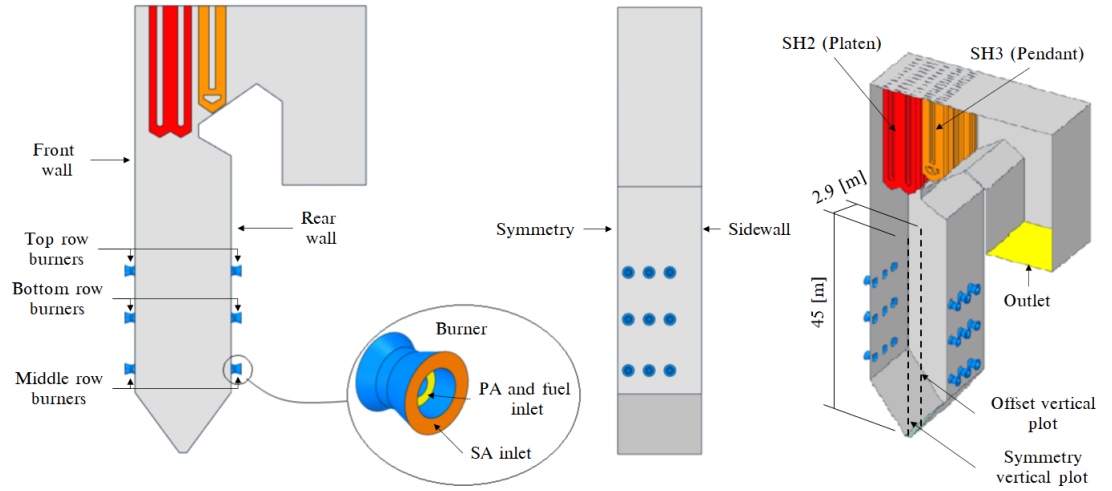


Figure 1: Boiler geometry and layout

The boiler furnace is fed by 6 mills, each supplying a pulverised fuel and primary air (PA) mixture to a burner row consisting of 6 burners. This mixture is injected through the inner burner annulus while the secondary air (SA) is fed through the outer annulus as seen figure 1.

The process model of the boiler configuration is shown in Figure 2. The process model includes all the heat exchanging components up till and downstream of the final SH, which include the secondary reheater (RH2), primary SH (SH1), primary reheater (RH1), economiser (EC) and the SA air heaters (SA-AH).

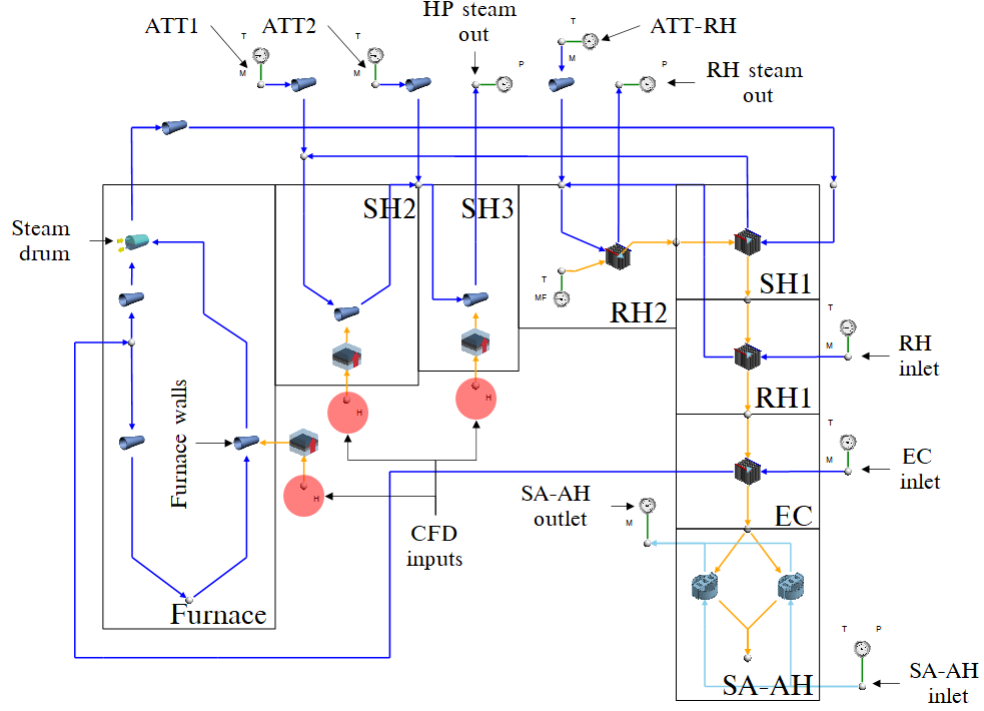


Figure 2: Process model of boiler set-up including the downstream convective components using Flownex SE 2021

3.2. Model inputs

Table 2 presents the coal characteristics utilized in the current study along with the coals higher heating value (HHV).

For a 32% boiler load the current operational protocol is the to use the bottom front and rear burner rows to meet the low-load demand. For this

Table 2: Utility boiler fuel characteristics

Fuel constituent	Fraction	Unit
<i>Ultimate analysis - (DAF)</i>	-	-
Carbon	0.7753	kg/kg_{fuel}
Hydrogen	0.0415	kg/kg_{fuel}
Nitrogen	0.0181	kg/kg_{fuel}
Oxygen	0.1474	kg/kg_{fuel}
Sulphur	0.0175	kg/kg_{fuel}
<i>Proximate analysis - (AR)</i>	-	-
Fixed carbon	0.340	kg/kg_{fuel}
Volatile matter	0.196	kg/kg_{fuel}
Ash	0.4090	kg/kg_{fuel}
Moisture	0.0550	kg/kg_{fuel}
Energy content - (DAF)	Value	
Higher heating value	15070	kJ/kg_{fuel}

study six cases are simulated in total with the following three burner firing configurations being utilized:

1. Bottom front and rear row burners are fired (Case 1 & Case 4)
2. Middle front and rear row burners are fired (Case 2 & Case 5)
3. Bottom front and middle rear row burners are fired (Case 3 & Case 6)

Two permutations of the SA flow rate, at the non-firing burners, are used for each of the firing configurations mentioned above. Table 3 shows the input conditions for cases 1 to 6. The data is the result of a boilers mass and energy balance calculations.

Table 3 shows a lower mass flow rate of SA air for case 4 to 6, this was done to compare the expected increase in boiler utilization efficiency, since less dry gas losses are expected, and the effects the drop in the flue-gas mass flow rate has on the convective pass components modelled in the process model.

Table 3: Case 1 to 6 model inputs on a per burner basis.

Active burners	Cases 1 - 3	Cases 4 - 6
Fuel flow rate [kg/s]	1.05	1.05
PA flow rate [kg/s]	4.95	4.95
SA flow rate [kg/s]	14.85	14.85
Non firing burners		
SA flow rate [kg/s]	5	2.5
Input air temperatures		
PA [K]	373	373
SA [K]	520	510

3.3. Numerical solution strategy

170 The CFD simulations were performed using ANSYS Fluent v19.5[®] pressure-based solver. the pressure-momentum coupling utilised the SIMPLE technique. Second-order upwinding was used to discretize the momentum, energy and species equations, whereas PRESTO! was used to discretize the pressure equation. The scalar field equations used a second-order upwind scheme.

175 The spatial discretization for all fields (except pressure) was set to first-order upwind for the first 1000 iterations to ensure a stable solution, after which the discretization order was increased to the above mentioned criteria. For all cases the maximum mass imbalance was 0.024 [kg/s] for a total gas flow rate of 190 [kg/s] and a heat imbalance of 1770 [kW] for a total heat input of 283 [MW].

180 The remaining fields were solved till convergence.

The operating protocol of the case study boiler requires that burners which are not firing to inject SA air at a rate of 5 [kg/s], this is to maintain non-firing burner integrity.

4. Results & discussion

185 The current section will discuss the results obtained from using the above-mentioned modelling methodologies. The validity of the modelling approach will first be established by comparing the simulation results for MCR load cases (namely 100%, 81% and 60% MCR loads) to that of the experimentally obtained results of the actual plant. Once the model has been shown to demon-
190 strate sufficient accuracy in determining the overall heat loads and combustion characteristics in the boiler furnace at varying loads, the results of the various low-load burner firing configurations are shown and discussed.

4.1. Model validation

The validation of the proposed model was conducted for three steady-state
195 MCR loads of 100%, 80% and 60%. The model inputs and boundary conditions can be obtained from the study conducted by Laubscher and Rousseau [3], where using the same boiler of the present study, they evaluated the thermal performance of the heat exchanging components at full and reduced boiler loads.

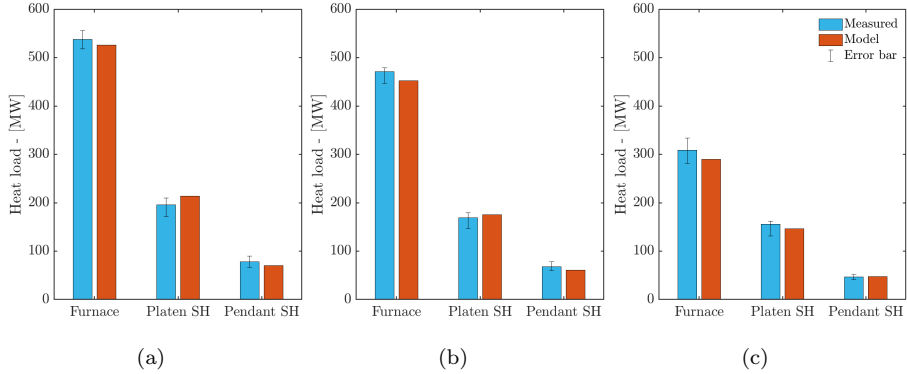


Figure 3: Comparison of experimentally calculated and model heat loads for the furnace, platen SH and pendant SH at (a) 100% MCR, (b) 80% MCR and (c) 60% MCR

In figure 3 it is shown that the overall heat loads are in good agreement
200 with the measured results. For the simulated validation loads the proposed

model results are within the associated error band, the general trend is an under prediction on the furnace heat loads and an over prediction on the platen super-heater. The pendant super heater illustrate the best comparable results for all load cases.

205

The CFD model was further validated by comparing the CO_{ppm} and X_{O_2} measurements against the CFD results. The probe measurements were taken at a furnace height of 37.5 [m] near the center of the boiler during a full load (100% MCR) operating conditions. The probe is inserted from the side walls to
 210 a depth of 4.5 [m], measurements were taken every 0.5 [m] increment.

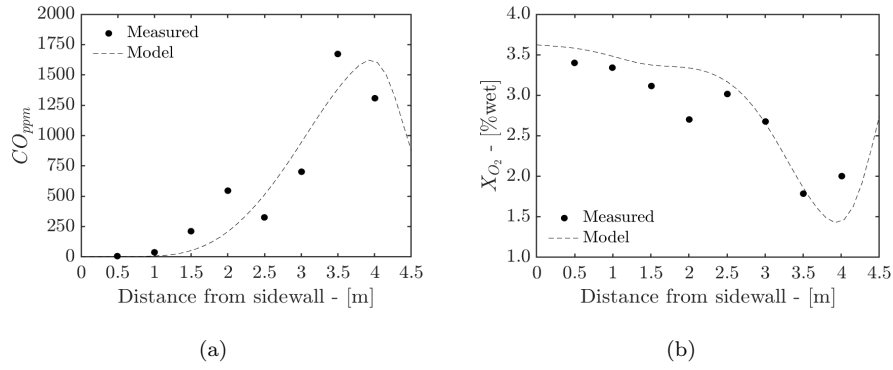


Figure 4: Experimentally calculated CO and O_2 concentration predictions

Figure 4 shows the averaged measurement values to that of the CFD predictions. It can be seen that the CFD model can sufficiently resolve the CO_{ppm} and X_{O_2} concentrations at the given probe location. For further information
 215 regarding the validation of the model the interested reader is directed to the works of Rawlins et al [REFERENCE]

4.2. Simulation results for various burner firing arrangements at 32% MCR

Explain the investigation table with case descriptions Need flownex model and process modelling description

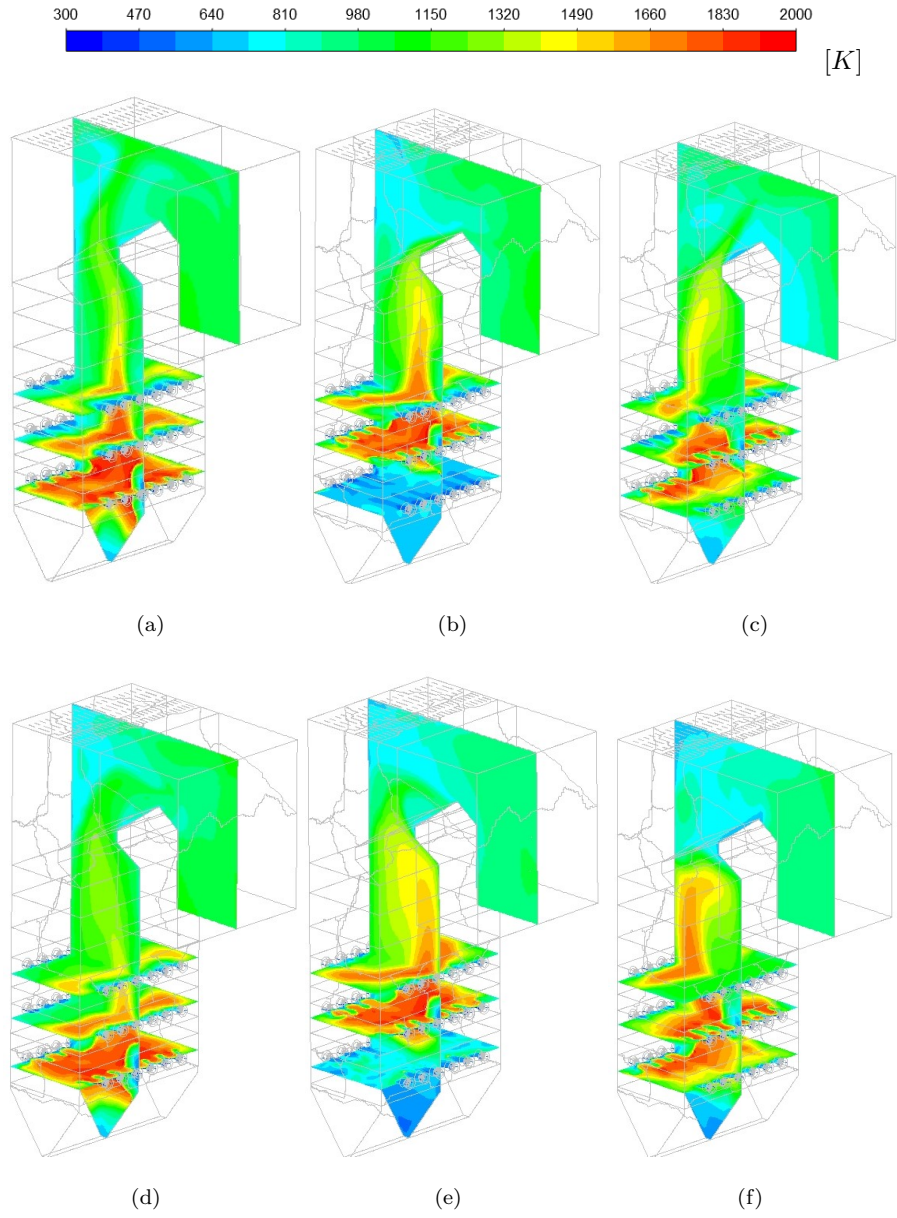


Figure 5: Temperature fields for cases 1 through 6 [(a)-(f)]

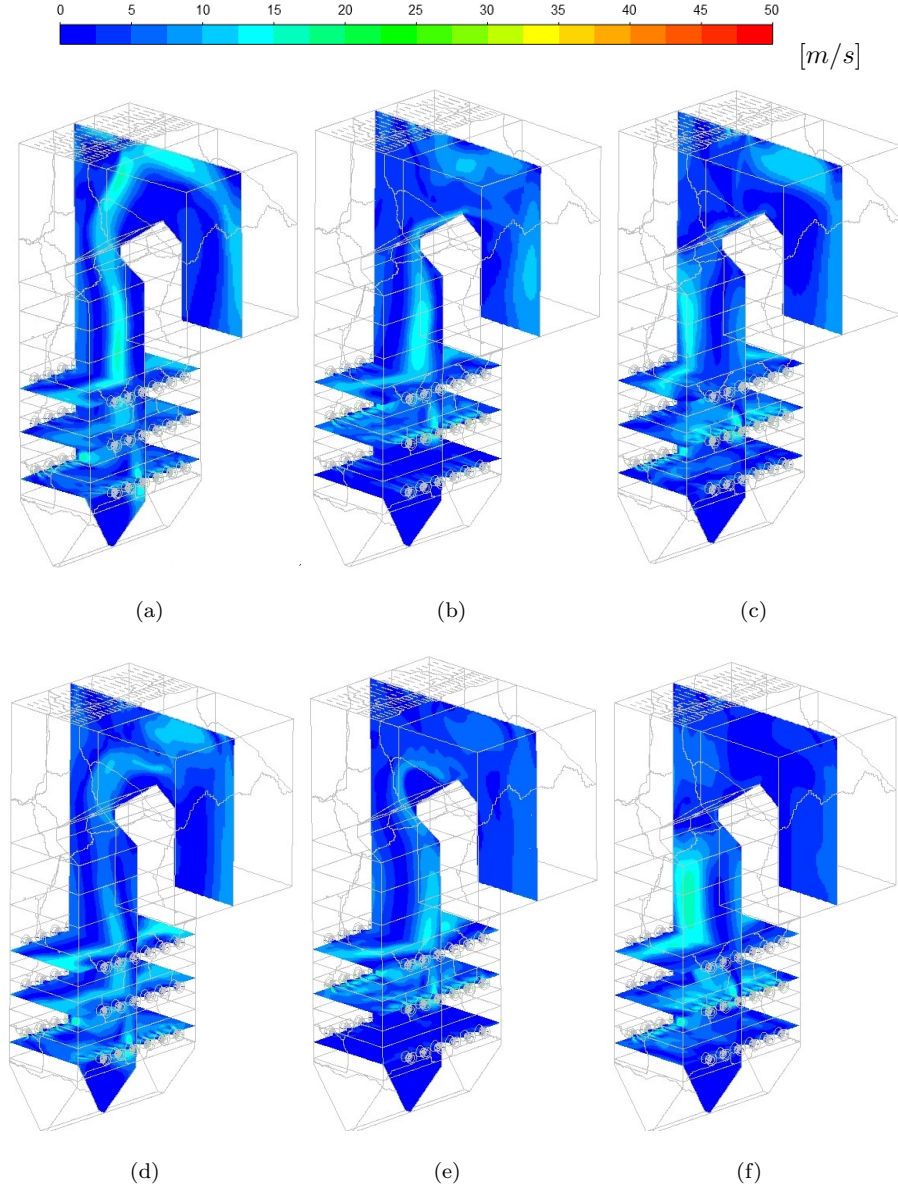


Figure 6: Velocity fields for cases 1 through 6 [(a)-(f)]

$$T_{metal} = T_{wall} - \left(\frac{\dot{q}_{SH} t_{ASH}}{\lambda_{ASH}} \right) \quad (23)$$

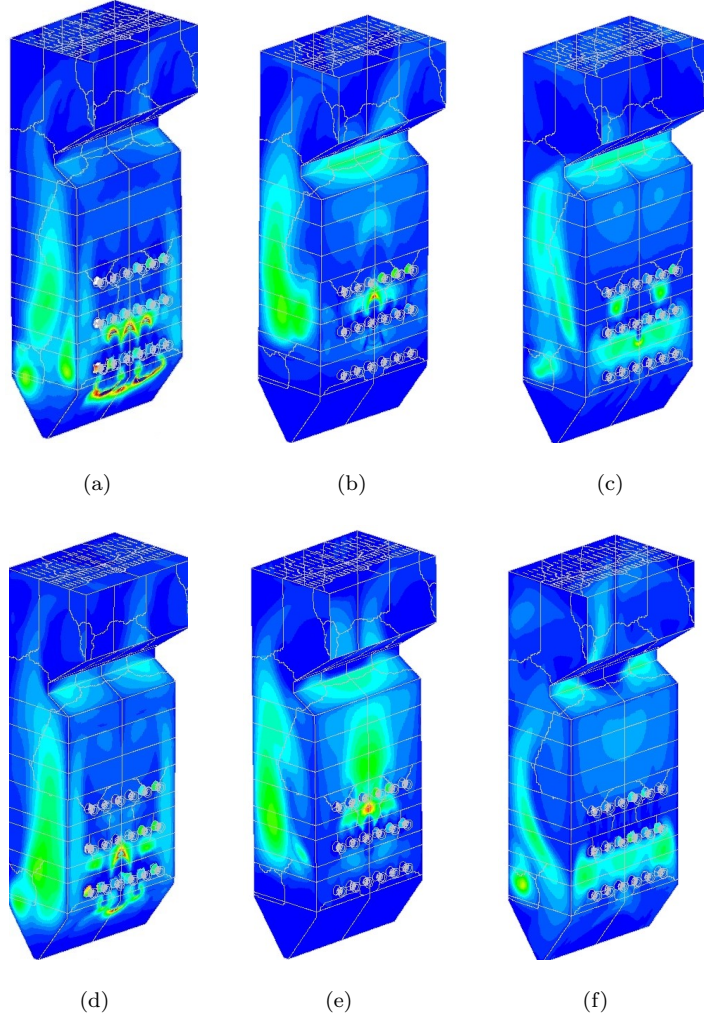
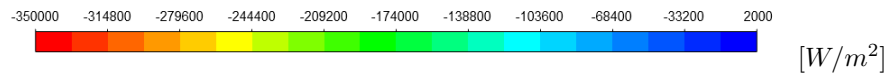


Figure 7: Heat fluxes profiles for cases 1 through 6 [(a)-(f)]

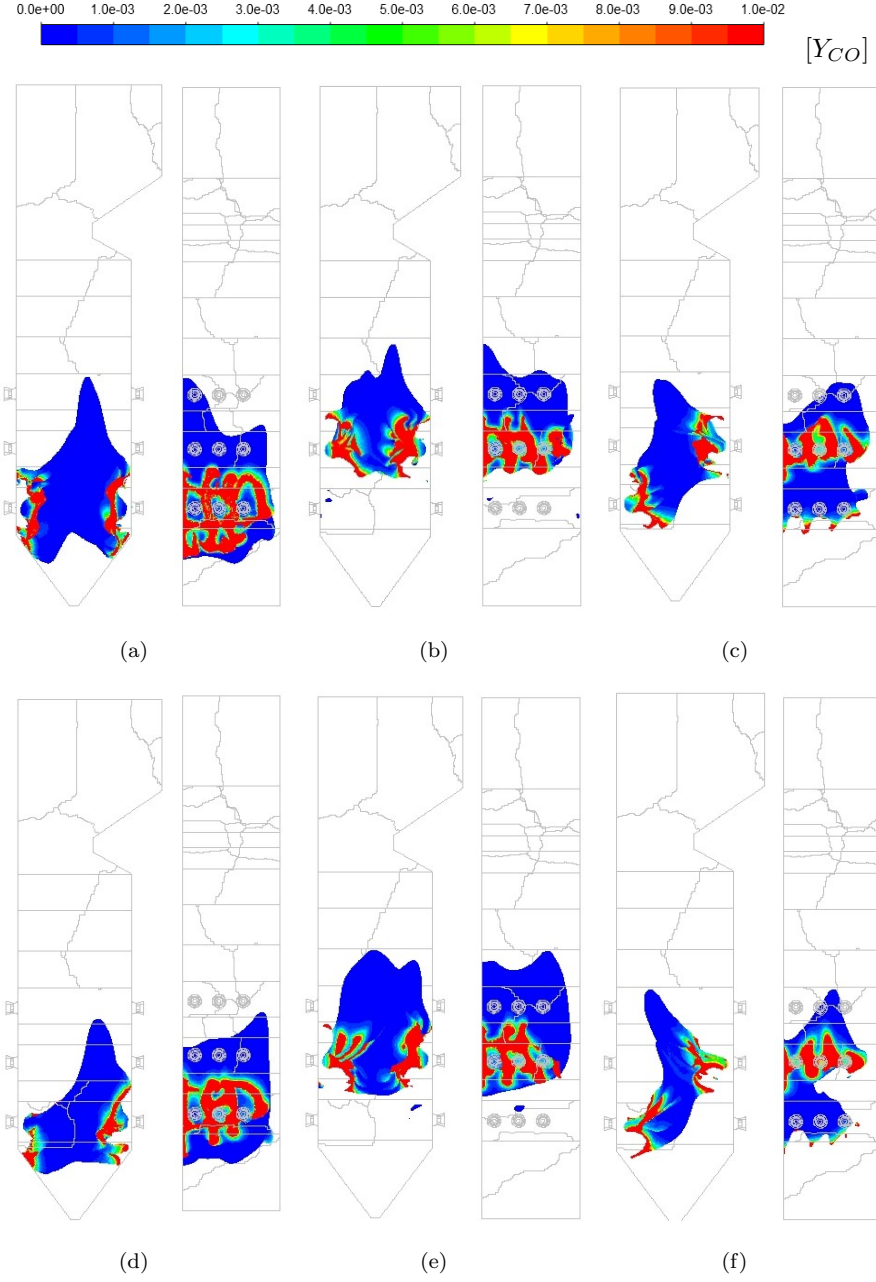


Figure 8: CO mass fraction (Y_{CO}) concentrations for cases 1 through 6 [(a)-(f)] on a temperature iso-surface of 1600 K

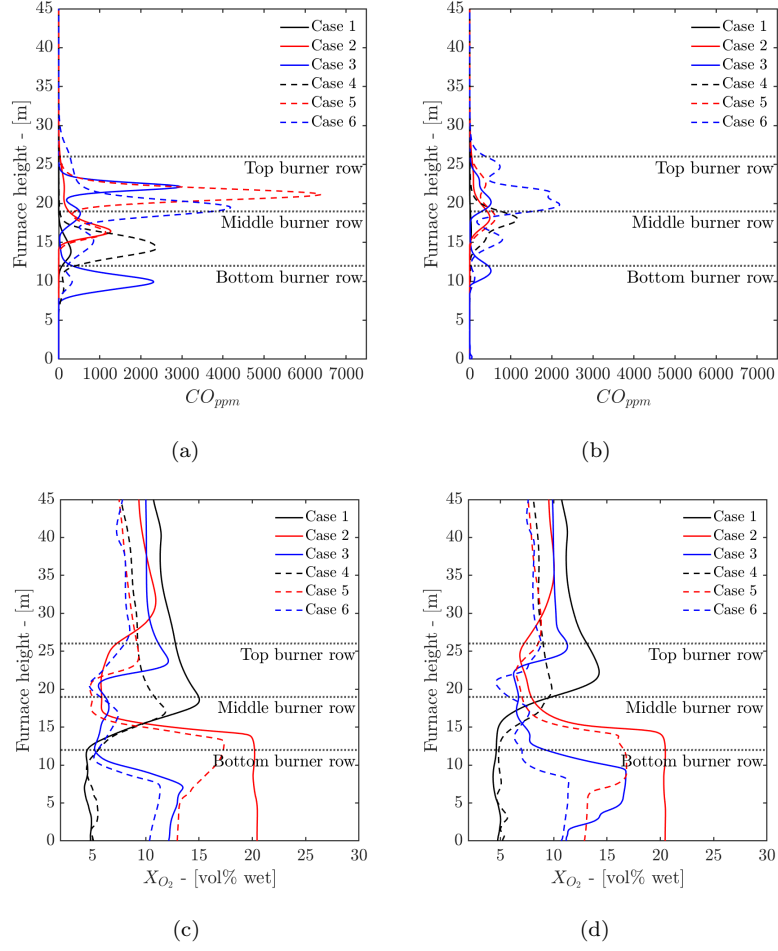


Figure 9: CO_{PPM} [(a) and (b)] and X_{O_2} [(c) and (d)] line plots on symmetry and offset vertical probe lines

Table 4: Process model control parameters

	Cases					
	1	2	3	4	5	6
Main steam flow rate [kg/s]	166	163	170	171	169	163
Main steam exit temp [$^{\circ}C$]	535	535	535	535	535	535
RH steam flow rate [kg/s]	150	148	154	154	153	147
RH steam exit temp [$^{\circ}C$]	535	535	535	535	520	490
Boiler efficiency [%]	86.2	84.9	88.8	88.2	86.6	82.2
Attemperator 1 [kg/s]	10.5	15	16	11.5	9.5	12
Attemperator 2 [kg/s]	5	8	5	4	5	5.5
Attemperator RH [kg/s]	0.5	1	1	0	0	0

Table 5: Furnace exit conditions and SH wall temperatures

	Cases					
	1	2	3	4	5	6
<i>Furnace exit</i>						
Exit temperature [K]	1168	1230	1215	1208	1306	1298
Unburnt carbon [$(\times 10^{-3})\%$]	1.83	1.94	1.54	1.81	1.89	1.62
<i>Platen SH</i>						
Max wall temperature [K]	754	750	765	766	753	763
Mean wall temperature [K]	726	712	719	727	715	724
<i>Pendant SH</i>						
Max wall temperature [K]	805	807	811	808	800	802
Mean wall temperature [K]	793	788	792	795	788	784

Table 6: Radiative heat transfer percentage for the platen and pendant SH

	Cases	
	3	6
Evaporator		
Platen SH [%]		
Pendant SH [%]		
Secondary RH [%]		
Primary SH [%]		
Primary RH [%]		
Economiser [%]		

220 5. Conclusions

Acknowledgements

The authors would like to thank the Eskom EPPEI program for financially supporting the present study and acknowledge the computational resources provided by the Centre for High Performance Computing (CHPC), South Africa.

225 References

References

- [1] A. Dugum, K. Hanjalić, Numerical simulation of coal-air mixture flow in a real double-swirl burner and implications on combustion anomalies in a utility boiler, *Energy* 170 (2019) 942–953. doi:10.1016/j.energy.2018.12.121.
- [2] Eskom Power Generation (2017).
URL <http://www.eskom.co.za/Whatweredoing/ElectricityGeneration/Pages/Electricity{ }Generation.aspx>
- [3] R. Laubscher, P. Rousseau, CFD study of pulverized coal-fired boiler evaporator and radiant superheaters at varying loads, *Applied Thermal Engineering* 160. doi:10.1016/j.applthermaleng.2019.114057.
- [4] B. Hernik, W. Zablocki, Numerical research of combustion with a minimum boiler load, *Archives of Thermodynamics* 41 (4) (2020) 93–114. doi:10.24425/ather.2020.135855.
- [5] J. Chang, X. Wang, Z. Zhou, H. Chen, Y. Niu, CFD modeling of hydrodynamics, combustion and NO_x emission in a tangentially fired pulverized-coal boiler at low load operating conditions, *Advanced Powder Technology* 32 (2) (2021) 290–303. doi:10.1016/j.appt.2020.12.008.
URL <https://doi.org/10.1016/j.appt.2020.12.008>

- 245 [6] N. Modliński, K. Szczepanek, D. Nabagło, P. Madejski, Z. Modliński, Mathematical procedure for predicting tube metal temperature in the second stage reheater of the operating flexibly steam boiler, *Applied Thermal Engineering* 146 (October 2018) (2019) 854–865. doi:10.1016/j.applthermaleng.2018.10.063.
- 250 [7] R. Laubscher, P. Rousseau, Numerical investigation into the effect of burner swirl direction on furnace and superheater heat absorption for a 620 MWe opposing wall-fired pulverized coal boiler, *International Journal of Heat and Mass Transfer* 137 (2019) 506–522. doi:10.1016/j.ijheatmasstransfer.2019.03.150.
- 255 [8] J. Gu, Q. Liu, W. Zhong, A. Yu, Study on scale-up characteristics of oxy-fuel combustion in circulating fluidized bed boiler by 3D CFD simulation, *Advanced Powder Technology* 31 (5) (2020) 2136–2151. doi:10.1016/j.appt.2020.03.007.
URL <https://doi.org/10.1016/j.appt.2020.03.007>
- 260 [9] Y. Du, C. Wang, Q. Lv, D. Li, H. Liu, D. Che, CFD investigation on combustion and NOx emission characteristics in a 600 MW wall-fired boiler under high temperature and strong reducing atmosphere, *Applied Thermal Engineering* 126 (x) (2017) 407–418. doi:10.1016/j.applthermaleng.2017.07.147.
265 URL <http://dx.doi.org/10.1016/j.applthermaleng.2017.07.147>
- [10] J. Fan, L. Qian, Y. Ma, P. Sun, K. Cen, Computational modeling of pulverized coal combustion processes in tangentially fired furnaces, *Chemical Engineering Journal* 81 (1-3) (2001) 261–269. doi:10.1016/S1385-8947(00)00212-6.
- 270 [11] S. Chen, B. He, D. He, Y. Cao, G. Ding, X. Liu, Z. Duan, X. Zhang, J. Song, X. Li, Numerical investigations on different tangential arrangements of burners for a 600 MW utility boiler, *Energy* 122 (x) (2017) 287–300. doi:10.1016/j.energy.2017.01.093.

- [12] B. He, L. Zhu, J. Wang, S. Liu, B. Liu, Y. Cui, L. Wang, G. Wei, Computational fluid dynamics based retrofits to reheater panel overheating of No. 3 boiler of Dagang Power Plant, *Computers and Fluids* 36 (2) (2007) 435–444. doi:10.1016/j.compfluid.2005.09.005.
- [13] Y. Jiang, B.-H. Lee, D.-H. Oh, C.-H. Jeon, Optimization of operating conditions to achieve combustion stability and reduce NO_x emission at half-load for a 550-MW tangentially fired pulverized coal boiler, *Fuel* 306 (February) (2021) 121727. doi:10.1016/j.fuel.2021.121727.
URL <https://doi.org/10.1016/j.fuel.2021.121727>
- [14] S. Belošević, I. Tomanović, N. Crnomarković, A. Milićević, Full-scale CFD investigation of gas-particle flow, interactions and combustion in tangentially fired pulverized coal furnace, *Energy* 179. doi:10.1016/j.energy.2019.05.066.
- [15] F. Alobaid, N. Mertens, R. Starkloff, T. Lanz, C. Heinze, B. Epple, Progress in dynamic simulation of thermal power plants, *Progress in Energy and Combustion Science* 59 (2017) 79–162. doi:10.1016/j.pecs.2016.11.001.
URL <http://dx.doi.org/10.1016/j.pecs.2016.11.001>
- [16] R. Laubscher, P. Rousseau, Numerical investigation on the impact of variable particle radiation properties on the heat transfer in high ash pulverized coal boiler through co-simulation, *Energy* 195 (2020) 117006. doi:10.1016/j.energy.2020.117006.
URL <https://doi.org/10.1016/j.energy.2020.117006>
- [17] C. Yu, W. Xiong, H. Ma, J. Zhou, F. Si, X. Jiang, X. Fang, Numerical investigation of combustion optimization in a tangential firing boiler considering steam tube overheating, *Applied Thermal Engineering* 154 (2) (2019) 87–101. doi:10.1016/j.applthermaleng.2019.03.074.
URL <https://doi.org/10.1016/j.applthermaleng.2019.03.074>

- [18] V. Ranade, D. Gupta, Computational modeling of pulverized coal fired boilers, 1st Edition, Taylor & Francis, Boca Raton, 2015.
- [19] C. Sheng, B. Moghtaderi, R. Gupta, T. F. Wall, A computational fluid
 305 dynamics based study of the combustion characteristics of coal blends in
 pulverised coal-fired furnace, Fuel 83 (11-12) (2004) 1543–1552. doi:10.
 1016/j.fuel.2004.02.011.
- [20] M. Baum, P. Street, Predicting the combustion behaviour of coal particles,
 Combustion science and Technology 3 (43) (1971) 231.
- 310 [21] H. Knaus, U. Schnell, R. Klaus, On the modelling of coal combustion in a
 550MWe coal fired utility boiler, Progress in Computational Fluid Dynam-
 ics 1 (2001) 194–207.
- [22] A. C. Benim, B. Epple, B. Krohmer, Modelling of pulverised coal com-
 bustion by a Eulerian-Eulerian two-phase flow formulation, Progress in
 315 Computational Fluid Dynamics 5 (6) (2005) 345–361. doi:10.1504/PCFD.
 2005.007067.
- [23] H. Versteeg, W. Malalasekera, Introduction to Computational Fluid Dy-
 namics, The finite volume method, 2nd Edition, Pearson Prentice Hall,
 2007. doi:10.1002/9781119369189.
- 320 [24] W. Vicente, S. Ochoa, J. Aguilón, E. Barrios, An Eulerian model for the
 simulation of an entrained flow coal gasifier, Applied Thermal Engineering
 23 (15) (2003) 1993–2008. doi:10.1016/S1359-4311(03)00149-2.
- [25] J. Cai, M. Handa, M. F. Modest, Eulerian-Eulerian multi-fluid methods
 for pulverized coal flames with nongray radiation, Combustion and Flame
 325 162 (4) (2015) 1550–1565. doi:10.1016/j.combustflame.2014.11.023.
 URL <http://dx.doi.org/10.1016/j.combustflame.2014.11.023>
- [26] P. Basu, C. Kefa, L. Jestin, Boilers and burners: Design and theory, 1st
 Edition, Springer, New York, 2000.

- [27] M. F. Modest, Radiative Heat Transfer, 3rd Edition, Academic Press,
330 Kidlington, Oxford, U.K., 2013. doi:10.1016/j.neuroscience.2014.03.
010.
- [28] T. Smith, Z. Shen, J. Friedman, Evaluation of Coefficients for the Weighted
Sum of Gray Gases Model, Journal of Heat transfer 104 (1982) 602–608.
- [29] F. Lockwood, S. Rizvi, N. Shah, Comparative predictive experience of coal
335 firing, Proceedings of the Institution of Mechanical Engineers 200 (1986)
79–87. doi:10.1243/PIME.
- [30] C. Yin, On gas and particle radiation in pulverized fuel combustion fur-
naces, Applied Energy 157 (2015) 554–561. doi:10.1016/j.apenergy.
2015.01.142.
340 URL <http://dx.doi.org/10.1016/j.apenergy.2015.01.142>